C h a p t e r 5

On the Mechanism of Photodriven Hydrogenations of N_2 and Other Substrates by Hantzsch Ester: Buffer is Key to Generation of Reactive H-atom Donors

5.1 Introduction

The utility of proton-coupled electron transfer (PCET) in small molecule reductions (e.g., N_2) and organic transformations has motivated the development of reagents and catalysts with weak (net) X−H bonds capable of driving the reductive protonation of substrates.[1,2,3,4,5] Photoinduced weakening of X–H bonds offers a promising strategy; following excitation the X–H bond dissociation free energy ($BDFE_{X–H}$) can decrease dramatically, converting unreactive X−H bonds into potent H-atom donors (Figure 5.1A).[6,7] Model studies have for example demonstrated such reactivity via ruthenium photosensitizers with acidic ligands[8,9] and photoexcited metal hydrides.[10] Further, this strategy has recently been utilized in catalytic systems with H_2,[11,12,13] or $H^+/e^–$ equivalents derived from an acid and an electrode (Figure 5.1A).[14] While these strategies show promise, it remains a challenge to photogenerate species featuring highly reactive $H^+/e^–$ equivalents with sufficiently long lifetimes to facilitate PCET to highly unactivated substrates, such as N_2, unactivated alkenes, carbonyls, or CO.

Recently, our laboratory,[15] followed closely by a report from Nishibayashi and coworkers,[16] introduced photocatalytic N_2R using a well-defined synthetic system. In our study, catalytic blue-light-driven transfer hydrogenation of N_2 to 2 NH_3 (i.e., nitrogen reduction, N_2R) using 3 equivalents of the Hantzsch ester (HEH_2) as a source of the $H^+/e^–$ equivalents required for this transformation. An N_2R catalyst, $PNPMoBr_3$ ([$MoBr_3$]; PNP, 2,6-bis(di-tert-butylphosphinomethyl)pyridine),[17,18] was used to activate N_2, but curiously a 1:1 mixture of [ColH]OTf:Col (Col-buffer; Col = 2,4,6-trimethylpyridine; Figure 5.1B) was needed for efficient N_2R. *While this specific reagent cocktail showed substantial N_2R activity even in the absence of a photoredox catalyst* (e.g., Ir), other dihydropyridines we have canvassed required the addition of a photoredox catalyst; addition of an Ir photoredox catalyst enhanced the N_2R reactivity with HEH_2 as well. The related Nishibayashi study focused on systems using a photoredox catalyst to facilitate N_2R.[16]

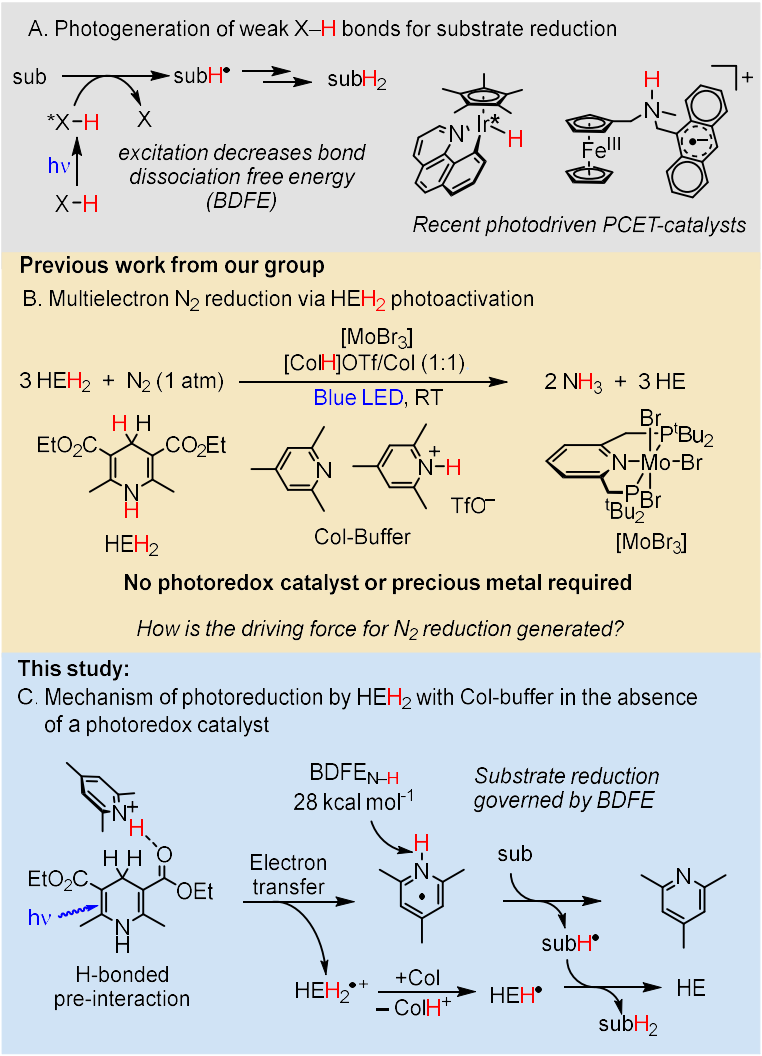

Figure 5.1. Photogenerated H-atom transfer reagents. (A) Photogeneration of PCET-donors for reductive reactions.[11,14] (B) Photodriven transfer hydrogenation for N_2R reduction with [$MoBr_3$], HEH_2, and Col-buffer.[15] (C) The mechanism proposed in this work for reduction by HEH_2 and Col-buffer.

The Mo-catalyst activates N_2 for proton-coupled reduction, but thermally driven N_2R with [$MoBr_3$] still requires a combination of highly reactive acids and reductants capable of generating (net) H-atom equivalents with effective bond dissociation free energy ($BDFE_{eff}$) of ~30 kcal mol^{-1}.[16,17,19,20] This corresponds to an overpotential of ~+65 kcal mol^{-1} per NH_3 formed. By contrast, a hypothetical dark reaction using HEH_2 has an overpotential of only +6 kcal mol^{-1}.[15]

Our prior report speculated that N_2R occurred via a mechanism similar to thermal N_2R by generating the required overpotential via irradiation of HEH_2 in the presence of Col-buffer. Specifically, we suggested that access to the reducing excited state of HEH_2 ($*HEH_2$) was critical for photodriven N_2R. Further, we suggested that $*HEH_2$ reduces [ColH]OTf to generate ColH$^{\bullet}$, a potent PCET donor. Here, we directly probe these hypotheses, providing evidence largely in support of the initially proposed scheme but also detailing how Col-buffer increases the photoreducing capacity of HEH_2 (Figure 5.1C).

Given the proposed role of HEH_2, it is useful to briefly review its photochemistry. The excited state of HEH_2 can be accessed by blue-light irradiation. Curiously, while the thermochemistry of $*HEH_2$ suggests it is a highly potent donor of e^- or H^+/e^- ($E(HEH_2^{\bullet+}/*HEH_2)$ = −2.5 V; $BDFE_{C–H}$ = −7 kcal mol^{-1}, Figure 5.2A),[21] its observed reactivity had previously been limited to activated organic substrates with extended electron-poor π-systems, e.g., nitroarenes,[22] imines,[23] α-bromoketones,[24] and electron-poor alkenes (Figure 5.2B).[25] This has been rationalized by the short lifetime and low quantum yield of $*HEH_2$ (Figure 5.2A).[24,26] The available data suggests that ground state pre-association between HEH_2 and substrate is required to observe substrate reduction; π-stacked, electron donor-acceptor (EDA) complexes between the electron-rich dihydropyridine and electron-poor aromatics are commonly invoked (Figure 5.2B). As such, substrate reduction is kinetically limited by the substrates' ability to form this pre-association complex, rather than the thermodynamics of HAT/ET from $*HEH_2$ to the substrate.

A contrast to the direct hydrogenation of substrates by HEH_2 is its use as a photoreductant in combination with R$^{\bullet}$-donors, such as Katritzky salts ($[^{2,4,6\text{-Ph}}PyrR]BF_4$)[27] or *N*-hydroxyphthalimide esters (Figure 5.2C).[28,29,30] Here, a π-stacked EDA complex forms between HEH_2 and the R$^{\bullet}$-donor. Irradiation results in electron transfer to release R$^{\bullet}$. As a pre-interaction between HEH_2 and substrate is not required in such a scenario, a wider range of substrates have been explored, e.g., Giese acceptors,[100] pyridines,[102] and Ni cross-coupling intermediates (Figure 5.2C).[101]

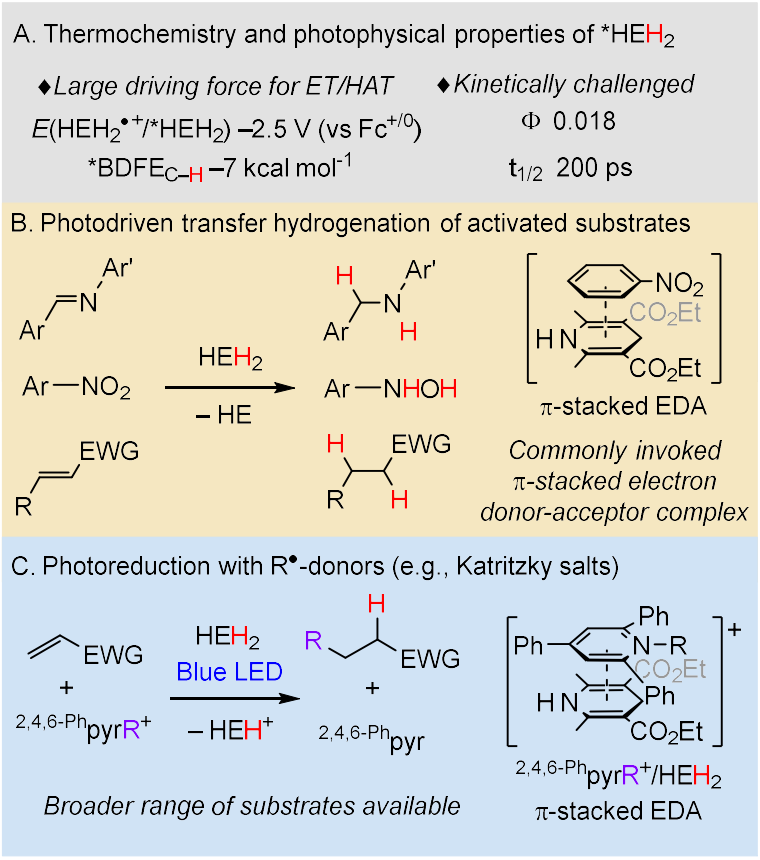

Figure 5.2. Overview of HEH_2 excited state properties and reactivity.[23,27,30]

Recent reports, including our previous study,[15] utilize HEH_2 as a photoreductant in transition metal or lanthanide-catalyzed reduction reactions where, based on the substrates, π-stacked EDA complexes are not likely operative.[31,32,33,34,35,36,37] However, despite the increasing utility of these HEH_2-driven photoreductions, limited mechanistic data hampers the development of new reactivity.[38]

Against this backdrop, we have interrogated the activation of HEH_2 by Col-buffer owing to its relevance to photodriven N_2R. A mechanism is mapped by addressing ground and excited state interactions of HEH_2 and buffer, and by monitoring the formation of organic radicals (Figure 5.1C). We find that an H-bonded adduct between $[ColH]^+$ and HEH_2 precedes the productive irradiation pathway. Following excitation of this associated pair, ET from HEH_2 to $[ColH]^+$ furnishes $ColH^•$. The latter is a potent H-atom donor ($BDFE_{N–H}$ = 28 kcal $mol^{–1}$). $[HEH_2]^{•+}$, the byproduct of this ET step, is deprotonated by

Col to generate the $HEH^{\bullet}$ radical and reforming $[ColH]^{+}$ as well. $HEH^{\bullet}$ serves as a second reactive H-atom donor. These pyridinyl radicals can reduce diverse substrates without the kinetic limitations observed by direct HEH_2 photoreductions.

5.2 Results

5.2.1 N_2R dependence on irradiation wavelength, buffer, and dihydropyridine

As noted, our previous report proposed blue light excitation of HEH_2 during photodriven N_2R. However, we had used broad (400-500 nm) LED lamps, which overlay with the UV-vis spectra of both HEH_2 and the $[MoBr_3]$ catalyst (Figure 5.3). To more reliably determine the photosensitized species during catalysis, we compared the N_2R reaction products at different irradiation wavelengths to the absorbance spectra of components of the catalytic reaction (akin to an action spectrum).[39]

Comparing the NH_3/Mo yield (Figure 5.3) at different wavelengths (Kessil™ LED H160 lamps at specific wavelengths; see Figure D.1 for emission spectra) to the UV-vis spectra of the reaction components, we find a relationship between N_2R and wavelength consistent with irradiation of HEH_2 (light blue trace, Figure 5.3) as a requisite to produce NH_3. Only when the strongly absorbing π-π* transition of HEH_2, with onset at ~435 nm (slightly red-shifted upon addition of Col-buffer, dark blue trace), is excited are the N_2R products NH_3 and oxidized Hantszch ester (HE, see Table D.2) observed. Specifically, we found that with loadings of 2.3 mM $[MoBr_3]$, 124 mM HEH_2, and 124 mM Col:[ColH]OTf in THF solvent, irradiating for 12 hours with 20 W at 427 nm and 440 nm reduced N_2 to NH_3 (6.6 ± 0.9 and 1.5 ± 0.5 equiv NH_3/Mo, respectively); no NH_3 was produced at 456 nm. While the overlap between the HEH_2 absorbance and the lamp emission spectra increases with lower wavelength across this series, $[MoBr_3]$ (yellow trace) absorbs similarly at 427, 440, and 456 nm. If $[MoBr_3]$ excitation is required for N_2R, such significant differences in NH_3 yield as a function of wavelength would not be expected. This conclusion is supported by the exploration of photodriven N_2R with a different precatalyst, $PCPMoCl_3$ (PCP = 1,3-bis((di-*tert*-butylphosphino)methyl)benzimidazol-2-

ylidene),[40] under otherwise identical conditions. The same trend is observed; N_2R occurs when irradiating at 440 or 427 nm but not at 456 nm (Table D.3).

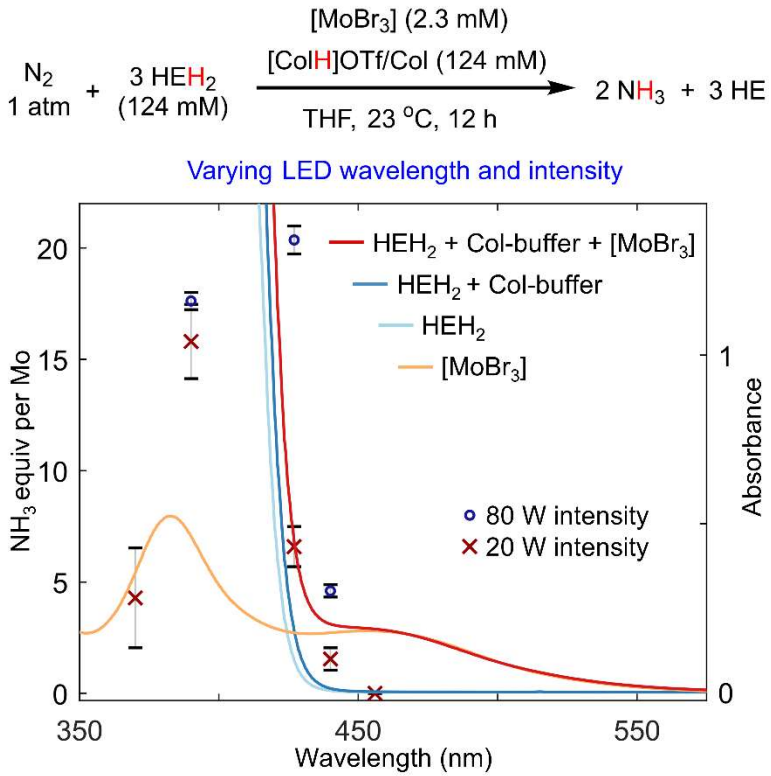

Figure 5.3. Plot of NH_3 yields per Mo at varying wavelengths (Black crosses and circles, left-hand axis) against the optical spectra of reaction components. Optical spectra were collected at catalytic concentrations in a 1 mm path length cuvette.

Oxidized Hantzsch pyridine (HE) is observed as the organic product for a balanced N_2R reaction. With [$MoBr_3$], when irradiating at 456 nm, only 12% of HEH_2 is converted to HE, consistent with the consumption of HEH_2 and N_2R being coupled. Further, irradiation at 440 nm at 20 W intensity for 12 hours results in incomplete consumption of HEH_2. Accordingly, when the light intensity and reaction time are increased (40 W, 24 hours), the NH_3 yields increase (4.6 ± 0.3 equiv NH_3/Mo). In this latter case, all of the HEH_2 was consumed, with about 85% recovered as HE. The amount of recovered HE is similar to what we previously reported using broader wavelength LEDs.[15]

Increasing the irradiation intensity at 427 nm (80 W, 12 hours) results in a substantial boost of the NH_3 yield (20.4 ± 0.6 equiv NH_3/Mo). These yields are more than

double those achieved in our previous report at the same catalyst and reagent loading, emphasizing the importance of irradiation wavelength and intensity. By lowering the catalyst loading (0.575 mM [$MoBr_3$]), the yields increase further to 28 ± 3 equiv NH_3/Mo, the highest yields achieved for molecular photodriven N_2R in the absence of precious metals (see Table D.1). Somewhat higher yields have been reported using a structurally related precatalysts, a Ir photocatalyst and a dihydroacridine organic H-atom donor.[16]

Lower wavelength light (390 nm light) shows high N_2R yields (15.8 ± 1.7 NH_3/Mo) even at low (20 W) intensity, consistent with more efficient excitation of HEH_2 (Figure D.18). However, increasing the intensity at this wavelength (80 W, 12 hours), only gives a slight boost in yield (17.6 ± 0.4 NH_3/Mo). A 390 nm irradiation, the HE yields decrease (HE recovered ~70%; Table D.2), suggesting increased side-reactivity, possibly via C−C coupling between HEH_2 and $ColH^+$. Still higher energy photons (370 nm) sharply decrease the NH_3 yield (4.3 ± 2.2 equiv/Mo). In addition to (likely) increased side-reactivity as deeper UV absorbances are excited, the excitation efficiency of HEH_2 drops at 370 nm.

We also explored a range of other buffers and dihydropyridines for photodriven N_2R, detailed in the Appendix D (see Figure D.2 and Table D.7). These studies established that any significant deviation of the structure of the Col-buffer or the dihydropyridine substantially attenuates NH_3 yields. The present study therefore focuses on the mechanism of HEH_2 activation by Col-buffer to understand how N_2R is facilitated by this particular combination of reagents.

5.2.2 Study of ground state interactions between HEH_2 and Col-buffer

Adding buffer to HEH_2 results in a red shift of the onset of the intense HEH_2 π-π* transition. The same shift is observed in the presence of just [ColH]OTf, but not Col alone, consistent with the primary interaction being between [ColH]OTf and HEH_2 (Figures 5.4A and D.15). Similar red-shifts have been observed upon the formation of π-stacked EDA complexes[22,100,101,41] or Lewis acid coordination to HEH_2 (presumably though the carbonyls).[35,42] This suggests two plausible pre-interaction scenarios between $[ColH]^+$ and HEH_2: H-bonding through the carbonyls, or π-stacking.

The HEH_2 ν(C=O) bands were probed (IR, 10 mM) as a function of added [ColH]OTf (0 to 160 mM, Figure 5.4B). A decrease in the intensity of the ν(C=O) bands at 1698 and 1685 cm^{-1} is observed as acid is added. New features grow in concomitantly; a blue-shifted feature appears at 1735 cm^{-1} and a red-shifted shoulder at ~1600 cm^{-1}. These shifts are consistent with H-bonding to one of the ester carbonyls, weakening this vibrational frequency, and in turn strengthening the other ν(C=O). A series of 4-phenyl substituted Hantzsch ester derivatives exhibits a similar splitting of vibrational modes in ethanol solvent (compared to solution state IR in aprotic solvents), albeit with a smaller magnitude.[43]

Computational methods (TPSS functional[44] def2-TZVP orbitals[45] using a CPCM to model the THF solvent[46]) provide additional insight into the pre-association of HEH_2 and $[ColH]^+$. Evaluating possible interactions, we find that while both arrangements are slightly disfavored over the free HEH_2/$[ColH]^+$, an H-bonded complex is favored over a π-stacking interaction ($\Delta G_{\text{H-bond}}$ = +1.3 kcal mol^{-1}, $\Delta G_{\pi\text{-stack}}$ = +3.5 kcal mol^{-1}; Figure 5.4C). For the H-bonded complex, time-dependent DFT (TD-DFT; a TPSSh functional[44] and def2-TZVP basis set[45]) calculations predict a red-shift in the UV-vis spectrum ($\Delta\lambda_{\text{abs, max, calc}}$ = + 4 nm; Figure D.78) as well as an increase in the vibrational frequency of one C=O mode ($\Delta\nu_{\text{calc}}$ = +7 cm^{-1}; Figure D.79) and decrease of the other mode ($\Delta\nu_{\text{calc}}$ = −40 cm^{-1}). In contrast, for the π-stacked EDA complex, the observed spectroscopic changes are not reproduced computationally: the optical spectrum predicts a low energy EDA band ($\lambda_{\text{abs, max, calc}}$ = 600 nm; Figure D.78) and a slight decrease of both vibrational modes ($\Delta\nu_{\text{calc}}$ =−2, −2 cm^{-1}; Figure D.79). Based on these experimental observations and computational predictions, we favor an H-bonded pre-association between HEH_2 and $[ColH]^+$.

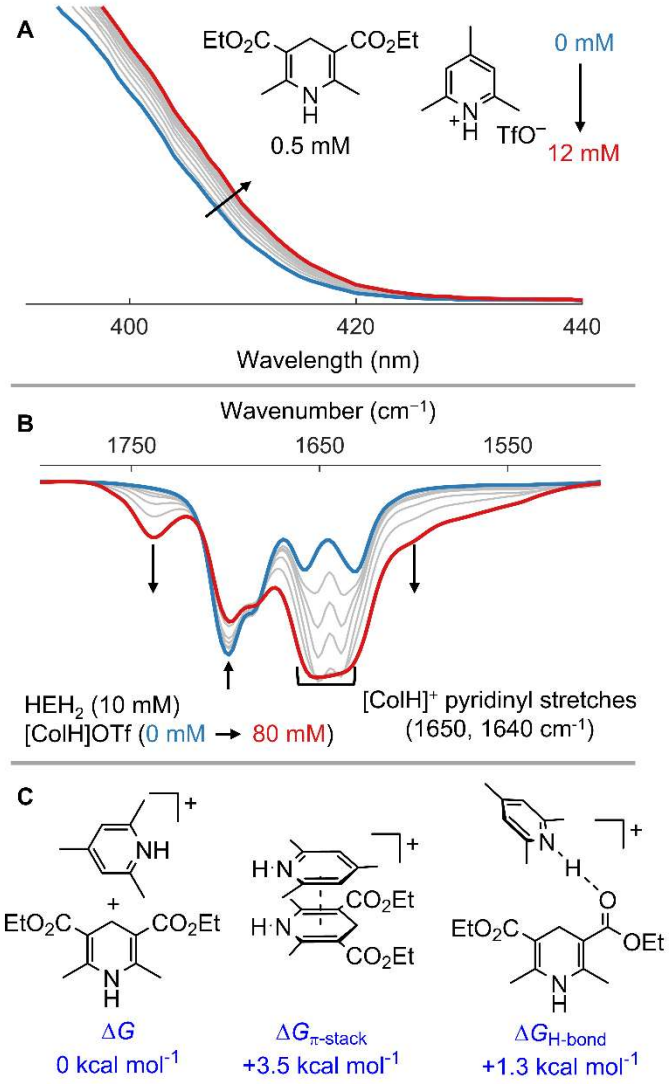

Figure 5.4. Study of ground-state interactions between HEH_2 and $[ColH]^+$. (A) UV-vis spectra of HEH_2 and [ColH]OTf. (B) Solution state infrared spectra of HEH_2 and $[ColH]^+$. (C) Computational analysis of possible pre-interaction complexes of HEH_2 and [ColH]OTf.

5.2.3 Photophysical studies

To study the interaction of Col-buffer with the excited state of HEH_2, we turned to photophysical measurements. Steady-state fluorescence spectroscopy data show that HEH_2 (in the absence of acid and base) is excited by $\lambda_{exc} < 430$ nm, with a distinct emission spectrum ($\lambda_{em\ max}$ at 455 nm, Figure 5.5A) and a low fluorescence quantum yield (0.018; Figure D.20). The excited state decay establishes a lifetime $t_{1/2} = 200$ ps (Figure D.23). The

short excited-state lifetime and low quantum yield match previous reports for HEH_2 in DMSO or MeCN.[24,26] The small Stokes shift and short lifetime are consistent with population of a singlet excited state, as has been observed in MeCN.[26]

The addition of [ColH]OTf red-shifts the excitation spectrum of HEH_2 slightly. In addition, substantial quenching is observed upon adding [ColH]OTf, yielding a Stern-Volmer[47] quenching constant of $K_{SV} = 22\ M^{-1}$ (Figure 5.5B and C). By contrast Col as base does not quench $*HEH_2$ or noticeably perturb the emission profile (Figure D.22).

$$\frac{I_0}{I_{[ColH(OTf)]}} \approx 1 + K_{SV}[ColH(OTf)] \quad \text{(eqn 5.1)}$$

$$K_{SV} = (K_{stat} + K_{dyn}) \text{ (eqn 5.2)}$$

The lifetime quenching effect of [ColH]OTf on $*HEH_2$ was measured to establish a small dynamic quenching constant $K_{dyn} = 1.4\ M^{-1}$ (Figure 5.5C, light blue line, and Figure D.25). Since this constant is an order of magnitude lower than the Stern-Volmer quenching constant (see eqn 5.1 and 5.2), the data point to $*HEH_2$ undergoing primarily static quenching by [ColH]OTf. To interrogate the initially formed product/s of $*HEH_2$ quenching by [ColH]OTf, we turned to transient absorption spectroscopy. The excitation of HEH_2 (1.2 mM) at 355 nm in the presence of [ColH]OTf (12 mM) was measured and shows the formation of a long-lived species ($\tau_{1/2}$ ~ 16 μs, Figure 5.6A, and C) with a maximum at 550 nm, and concomitant bleaching at 370 nm, consistent with HEH_2 consumption. This signal only forms in the presence of [ColH]OTf.

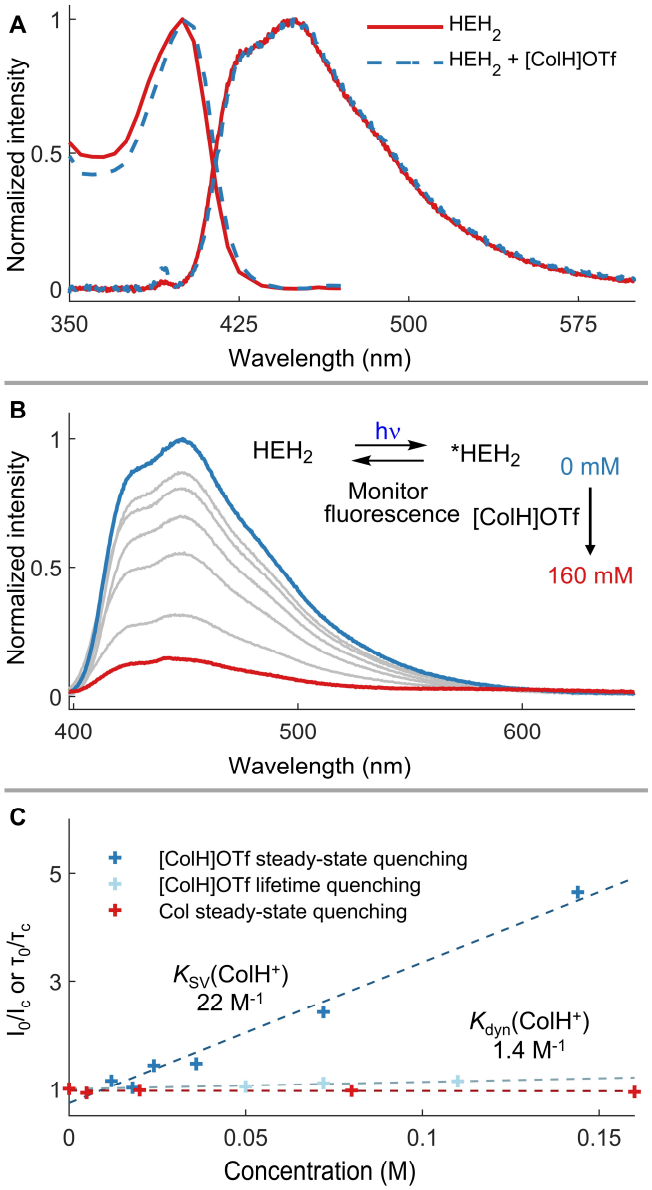

Figure 5.5. Steady-state fluorescence measurements of HEH_2 in the presence of [ColH]OTf. (A) Emission (Right) and excitation (left) spectra of HEH_2 (0.5 mM) in the absence (solid red) and presence of [ColH]OTf (20 mM, dashed blue). (B) Steady-state emission quenching of HEH_2 (0.5 mM) by [ColH]OTf (0 to 160 mM). (C) Steady-state and lifetime quenching plots of HEH_2 in the presence of [ColH]OTf and Col.

Based on time-dependent density functional theory (Figure D.82) predictions of the absorption spectra of several candidate organic species ($[HEH_2]^{\bullet+}$, $HEH^{\bullet}$, $^3HEH_2$, and $ColH^{\bullet}$), we find that the observed absorption is most consistent with assignment as

$[HEH_2]^{\bullet+}$ (red bars in Figure 5.6C). Dihydropyridine radical cations, albeit to our knowledge not $[HEH_2]^{\bullet+}$, have been generated via similar flash-photolysis experiments in the presence of electron acceptors, with transient absorption maxima ranging from 550-650 nm.[48,49,50]

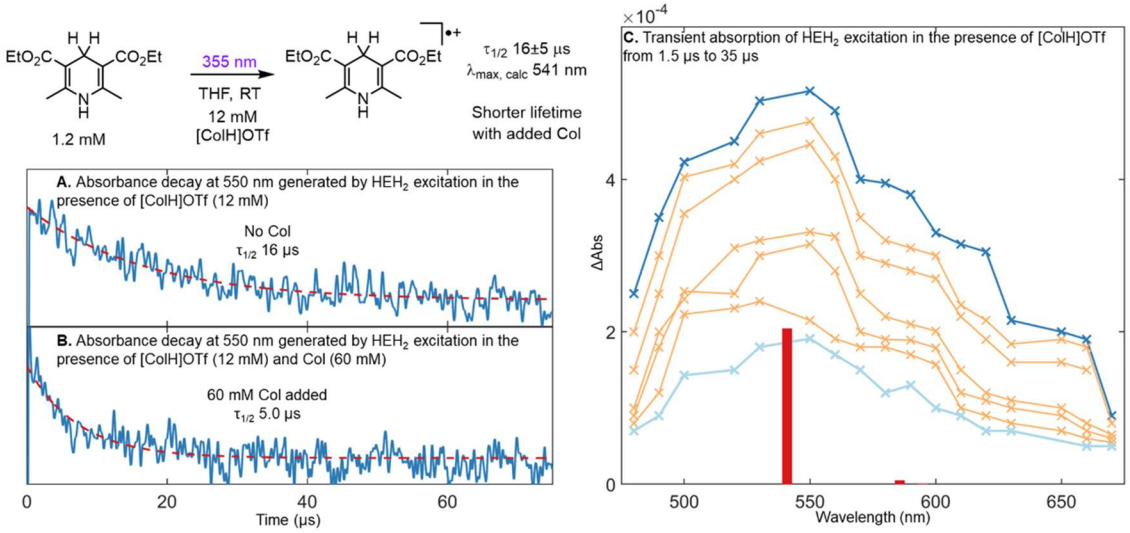

Figure 5.6. Transient absorption measurements of HEH_2 in the presence of [ColH]OTf and Col in THF. (A) Absorption decay of signal generated from HEH_2 (0.5 mM) in the presence of [ColH]OTf (12 mM) was monitored at 550 nm. (B) Same as A, but with added Col (60 mM). (C) TA spectrum of short-lived radical species. Intensity decreases from 1.5 μs (blue trace) to 35 μs. TD-DFT predicted absorbance maxima for $HEH_2^{\bullet+}$ at 541 and 586 nm, indicated by red bars.

In the presence of both [ColH]OTf and Col, we find that a similar signal decays faster (Figure 5.6B and Figure D.29). An explanation for this observation involves the deprotonation of $[HEH_2]^{\bullet+}$ by Col as a new decay pathway. Plotting the lifetimes as a function of base concentration allows determination of a deprotonation constant ($k = 2.4 \pm 0.6\ 10^6\ M^{-1}\ s^{-1}$; Figure D.40). This value matches data for previously reported deprotonations of dihydropyridine radical-cations.[50,51]

The formation of $[HEH_2]^{\bullet+}$ is readily rationalized by electron transfer from $^*HEH_2$ to [ColH]OTf, which would also furnish ColH$^{\bullet}$. Ground-state pre-association of HEH_2 with [ColH]OTf (vide supra) via a H-bond interaction sets the stage for ET. Following excitation, ET from $^*HEH_2$ ($E_{ox} = -2.5$ V) to the associated [ColH]OTf ($E_{red} = -2.0$ V)[52]

is favorable and would account for the static quenching pathway. Electron transfers through H-bonds are well precedented.[53,54,55]

In addition to observed ET from *HEH_2 we wondered if excited state proton transfer from *HEH_2 might play a role in catalysis. However, the excited state pK_a of HEH_2 was measured to 23.8 ± 0.9 in MeCN (see section A11), representing a weak acid, and in the context of this report a much weaker acid than the buffer ([ColH]OTf/Col, pK_a 15).[56]

5.2.4 Detection and characterization of photogenerated organic radicals by EPR spectroscopy

To study ground-state populations of organic species that may build up when HEH_2 and Col-buffer are irradiated, we turned to EPR spectroscopy. HEH_2 (100 mM), Col (100 mM), and [ColH]OTf (100 mM) in THF were irradiated with blue light and freeze-quenched after 1 minute and then analyzed by continuous-wave (CW) EPR. The data show formation of an $S = 1/2$ species with g = 2.002, consistent with an organic radical (Figure 5.7A). While narrow and in low yield (~10 μM), the radical is also characterized by a diagnostic apparent sextet (Figure 5.7B) in the 2nd derivate spectra. The intensity and spectral shape are unchanged upon varying the time of freeze-quenching (1 to 60 minutes; Figure D.42); both light and HEH_2 were required to observe any signal. While signals attributable to organic radicals could also be observed in the absence of Col-buffer, these had lower intensity and were distinct from those generated by HEH_2 and Col-buffer (Figure D.43). The apparent sextet can be formed in either toluene or 2-MeTHF, implying this signal is not related to the solvent (Figure D.46).

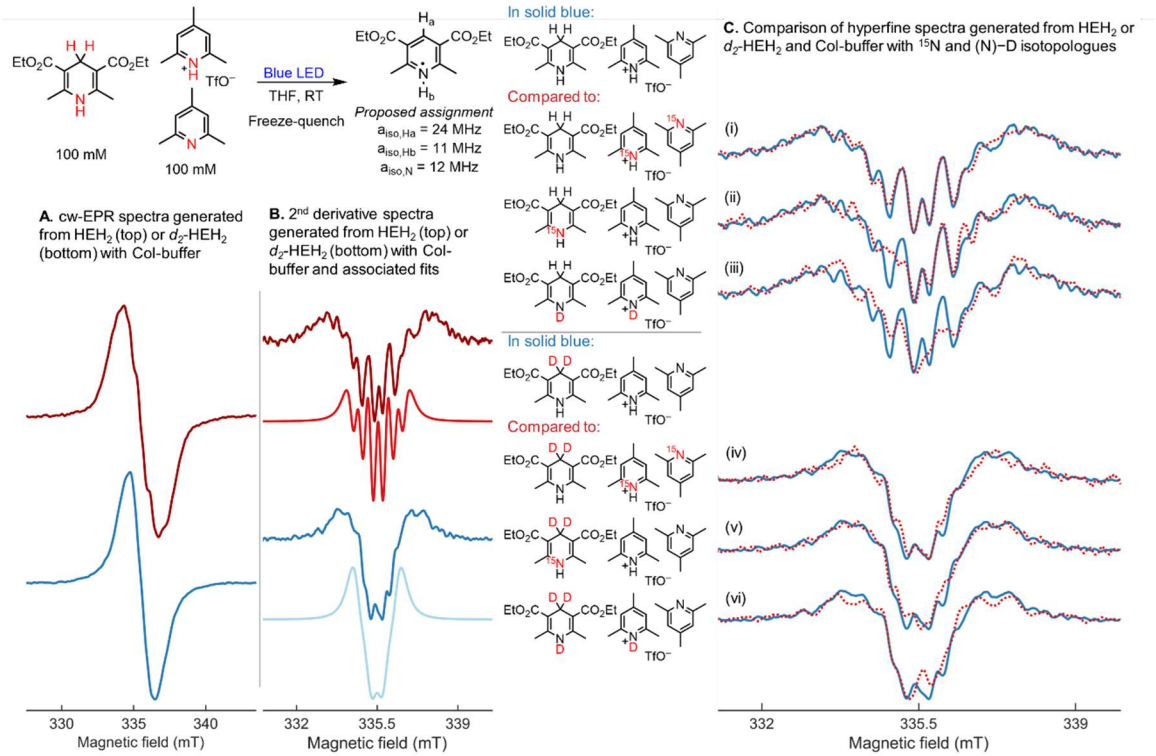

Figure 5.7. EPR detection of organic radicals. (A) CW-EPR spectra generated by irradiating HEH_2 or d_2-HEH_2 (100 mM) with Col-buffer (100 mM). Red atoms have been isotopically labeled to aid the assignment of the observed organic radical(s). (B) 2nd derivative spectra from irradiating HEH_2 or d_2-HEH_2 (100 mM) with Col-buffer (100 mM). Fits generated from proposed parameters. (C) 2nd derivative spectra comparing ^{15}N labeling in either HEH_2 or Col-buffer, N−D labeling (both [ColD]OTf and d_1-HEH_2) and comparison of same isotopologues using d_2-HEH_2 (C_4-deuteration). Acquisition parameters: temperature = 77 K; MW frequency = 9.38 GHz; MW power = 2 mW; modulation frequency = 100 kHz; modulation amplitude = 0.1 mT; conversion time = 20.5 ms.

To aid assignment we synthesized a series of isotopologues, including ^{15}N-HEH_2, ^{15}N-Col buffer, d_2-HEH_2 (double deuterated at C_4−H positions), d_1-HEH_2 (N−H deuterated), [ColD]OTf, d_3-HEH_2, and ^{15}N-d_2-HEH_2. Spectra generated with d_2-HEH_2 show a collapse of much of the hyperfine structure, suggesting significant coupling to the C_4 H-atom(s) (Figure 5.7A and B). Other changes upon labeling were subtler but could be identified by careful comparison of 2nd derivative spectra (Figure 5.7B and C). Given the significant spectral change observed using d_2-HEH_2, comparison of labeled samples (^{15}N or N−D) to samples prepared with either natural abundance HEH_2 (Figure 5.7C, traces i-

iii) or d_2-HEH_2 (traces iv-vi) were used to confirm differences that might be observed more reliably. ^{15}N-labeling of either Col-buffer (traces i and iv) or HEH_2 (traces ii and v) demonstrated changes in the spectra only upon labeling HEH_2, suggesting an HEH_2-derived radical. We also observed changes in the 2nd derivative spectra upon N−D labeling, using both H and D-labeled at the C_4–H positions to confirm this (traces iii and vi).

To account for these observations and provide reasonable simulated fits, a species with coupling to two types of H atoms, one C_4–*H* (a_{iso} = 24 MHz) and one N−*H* (a_{iso} = 11 MHz), as well as coupling to the HEH_2 *N*-atom (a_{iso} =12 MHz) is proposed. The relative magnitudes of these values closely match previous hyperfine values measured for carbonyl-substituted pyridinyl radicals.[57,58] This analysis points to $HEH^{\bullet}$ as the species in question, expected following rapid deprotonation of $[HEH_2]^{\bullet+}$ invoked in the photophysical measurements discussed above.

5.2.5 Substrate reduction studies and benchmarking the effective driving force for H-atom delivery by irradiation of HEH2 and Col-buffer

The spectroscopic data discussed above suggests that irradiation of HEH_2 in the presence of Col-buffer generates $HEH^{\bullet}$ and (by implication) $ColH^{\bullet}$. These pyridinyl radicals serve as potential donors of H-atom equivalents to Mo-bound N_2R intermediates ($Mo–N_xH_y$), and other substrates. Unsaturated organic substrates can allow for estimation of the driving force for net H-atom delivery; this motivated reactivity studies to calibrate the advantage of Col-buffer for chemical transformations beyond N_2R.

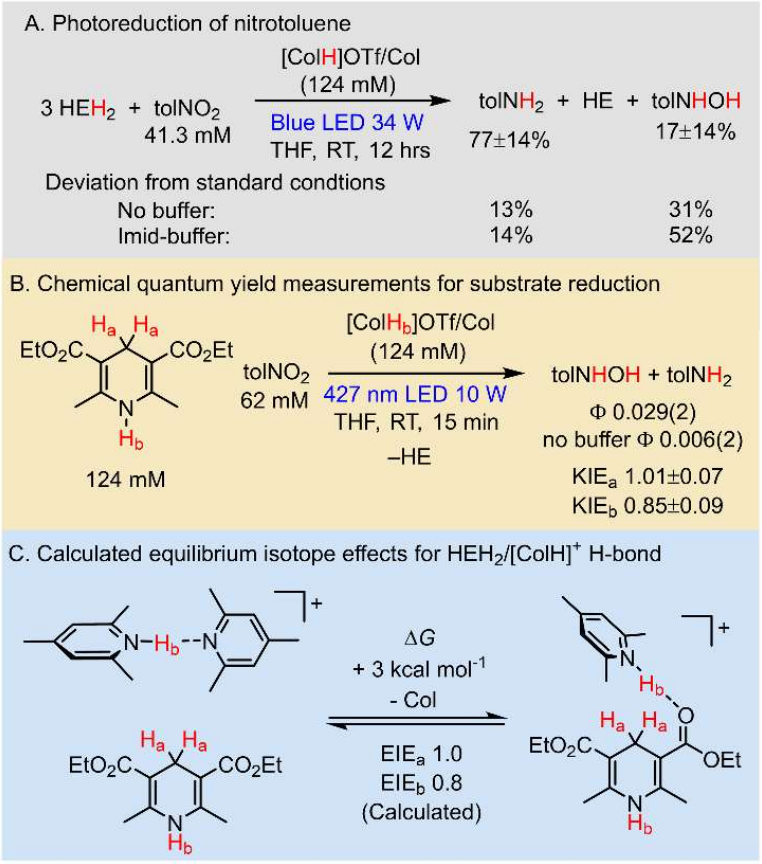

Figure 5.8. Photoreduction of $tolNO_2$ by HEH_2 and Col-buffer.

HEH_2 photoreductions are well established, though studies of these reactions in the presence of Brønsted acids or bases are rare;[25,59] the effects of Col-buffer on organic photoreductions by HEH_2 had not been explored. For the substrates examined here, HEH_2 photoreductions show improved yields and increased selectivity for more reduced products, with Col-buffer displaying distinct behavior. For example, the photoreduction of $tolNO_2$ (4-nitrotoluene) by HEH_2 in the absence of buffer occurs over 72 hours to yield primarily tolNHOH (4-tolyl hydroxylamine).[22] By contrast, irradiation of HEH_2 (124 mM) in the presence of $tolNO_2$ (41.3 mM, 0.33 equiv per HEH_2) and Col-buffer (124 mM) for just 12 hours furnished primarily aniline (2.7:1 ratio $tolNH_2$:tolNHOH, Figure 5.8A) and a high total yield of reduced products (97%). Using an imidazolium/imidazole buffer instead (Imid; pK_a 15.1 compared to pK_a 15.0 for Col in MeCN, Figure 5.8A)[56] furnished lower yields for reduced products and favored tolNHOH, pointing again to Col-buffer as special.

The chemical quantum yield for tolNO_2 reduction was determined to be 0.029(2) in the presence of Col-buffer. This value is greater than the measured fluorescence quantum yield of HEH_2 (0.018), intimating enhanced reactivity in the presence of Col-buffer (Figure 5.8B). The quantum yield for tolNO_2 reduction decreases fivefold in the absence of Col-buffer. Additionally, measurements of the quantum yield with the C_4–*H* (H_a ; Figure 5.8B) and N–*H* (H_b) deuterated isotopologues of HEH_2 and Col-buffer were performed to probe the kinetic isotope effects (KIE) for tolNO_2 reduction. Curiously, while there is no KIE using d_2-HEH_2 (deuterated C_4–H bonds, KIE_a 0.99 ± 0.06), N–D deuteration (d_1-HEH_2 and d_1-Col-buffer, KIE_b) shows a small, inverse KIE (0.84 ± 0.09).

Computational studies suggest that the proposed H-bonding pre-equilibrium between HEH_2 and Col-buffer can be used to rationalize these KIE data. By computation, the preferred conformation of HEH_2 and Col-buffer is free HEH_2 and an H-bonding homo-dimer $[ColH^{\cdots}Col]^+$.[60] However, the H-bond interaction of HEH_2 and $[ColH]^+$ is only slightly uphill (ΔG = 3.0 kcal mol^{-1}; Figure 5.8C). Shifting this equilibrium towards the H-bond interaction of HEH_2 and [ColH]OTf should favor substrate reduction. Thermodynamically, the proton (versus the deuteron) will favor the stronger H-bond of the $[ColH^{\cdots}Col]^+$ homo-dimer. Accordingly, computationally derived EIE_a and EIE_b (equilibrium isotope effects) provide values of 0.97 and 0.80, within the error of the experimentally measured KIEs for tolNO_2 reduction.

HEH_2 and Col-buffer are also competent for the reduction of other N–O bonds (Figure 5.9), including nitroalkanes ($^nPrNO_2$ to $^nPrNH_2$; 30 ± 5% yield per HEH_2), nitrate ($[NO_3]^-$ to NH_3, yield 35 ± 2% per HEH_2, confirmed by ^{15}N-labeling; Figure D.10), and amine N-oxides (Me_3N–O to Me_3N, yield 91 ± 5%). Electron-rich aromatic aldehydes $^{4\text{-}Me2N}$PhCHO and $^{4\text{-}MeO}$PhCHO can also be photoreduced by this approach, with the major product being a diol, consistent with radical addition of H• to the aldehyde to form the α-hydroxybenzyl radical, followed by bimolecular pinacol coupling. The low yields for pinacol coupling of aldehydes by HEH_2 in the absence of buffer is consistent with previous reports.[59] HEH_2 could not reduce less activated carbonyls, such as aliphatic ketones (benzylacetone), or activated aromatic esters (dimethylterphatalate), even with Col-buffer.

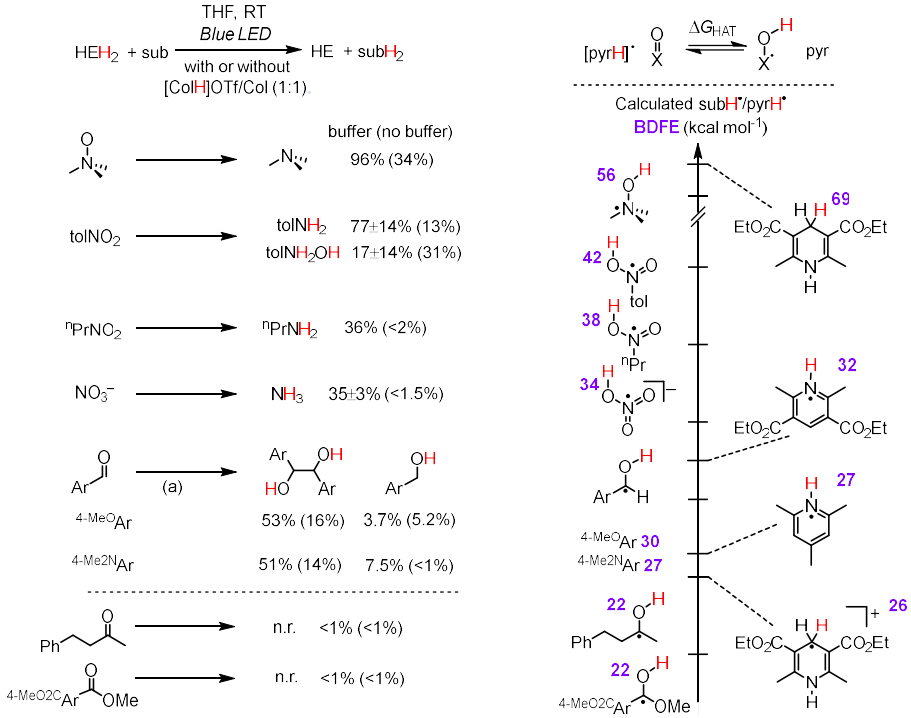

Figure 5.9. Photoreduction of organic substrates by HEH_2 (124 mM) and [ColH]OTf/Col (124 mM of each) in THF. All reactions run for 12 hours using Blue LED H150 lamps at 68 W except where noted. [a]Reaction run using H160 427 nm lamp (40 W) for 4 hours to minimize background reactivity. All yields given from the average of a minimum of two experiments.

This scope of substrates allows us to bracket the thermodynamic driving force for H^+/e^- transfer accessed by irradiation of HEH_2/Col-buffer. When analyzing the computationally derived $BDFE_{O–H}$ (TPSS def2-TZVP; Figure 5.9) following the addition of an H-atom to substrates, we find that only substrates with a sub–H$^\bullet$ $BDFE_{O–H,\ calc} \sim 27$ kcal mol^{-1} or higher can be reduced. This suggests that irradiation of HEH_2/Col-buffer generates a driving force for H^+/e^- transfer equivalent to a BDFE ~27 kcal mol^{-1}. This bond strength is comparable to some of the weakest isolable or *in situ* formed thermally generated PCET reagents.[61] Highly reactive photogenerated PCET donors have also been detailed.[11,14,62]

We find that the reactivity observed correlates closely with the weak BDFE calculated for [ColH]$^\bullet$ ($BDFE_{N–H,\ calc}$ = 27 kcal mol^{-1}) or $[HEH_2]^{\bullet+}$ ($BDFE_{N–H,\ calc}$ = 26 kcal mol^{-1}) as the donor/s of H-atoms during photoreduction. By contrast, other C/N–H bonds

that might be invoked in solution, such as HEH$^{\bullet}$ ($BDFE_{N-H,\ calc}$ = 32 kcal mol^{-1}, $BDFE_{estimated}$ = 41 kcal mol^{-1}, see section S11)[21] or HEH_2 ($BDFE_{N-H,\ calc}$ = 70 kcal mol^{-1}) feature stronger N/C−H bonds: these species should not be competent to reduce the less activated substrates, at least at the first H^+/e^- transfer step.

The role of $[HEH_2]^{\bullet+}$ ($BDFE_{N-H,\ calc}$ = 26 kcal mol^{-1}) as a potential PCET donor during irradiation cannot be ruled out (see Figure D.72 for a representative scheme). However, as $[HEH_2]^{\bullet+}$ is rapidly deprotonated by Col, we surmise this pathway is at most a minor contributor to substrate reduction, pointing to highly reactive [ColH]$^{\bullet}$ as the probable primary donor of H^+/e^-.

5.3 Discussion

The data obtained via this study allow us to propose a mechanistic outline by which HEH_2 and Col-buffer interact to reduce substrates. This is illustrated in Figure 5.10 via the elementary steps **a** to **h**.

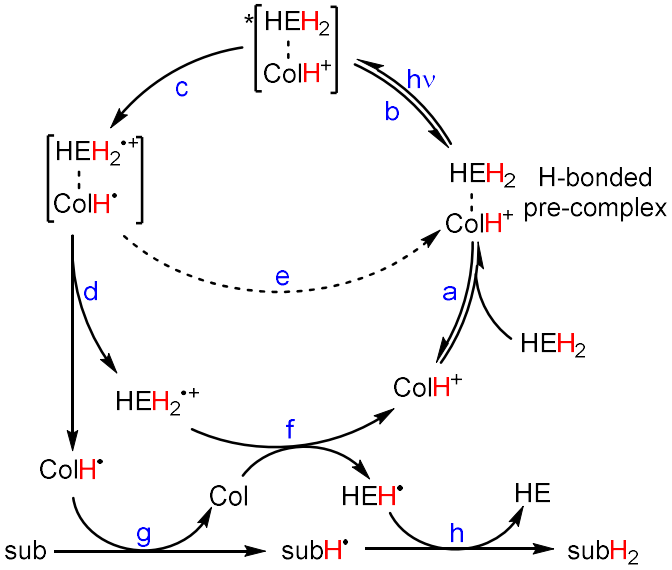

Figure 5.10. Proposed mechanism for 2 $H^+/2e^-$ reduction of substrates by HEH_2 mediated by Col-buffer with steps a-h labeled.

HEH_2 and [ColH]OTf associate via an H-bonded adduct (**a**) in a pre-equilibrium first step. Excitation (**b**) results in ET from *HEH_2 to [ColH]OTf to furnish the charge-transfer product (**c**), which then dissociates to release free ColH$^{\bullet}$ and $[HEH_2]^{\bullet+}$ (**d**). Back ET (BET, **e**) competes with this step but the reaction is driven forward by deprotonation of $[HEH_2]^{\bullet+}$

by Col to produce $HEH^{\bullet}$ and $[ColH]^{+}$ (**f**). Additionally, charge-transfer through an H-bonded complex may present a distinct advantage to the forward process. Following the ET step the H-bond strength should decrease; $ColH^{\bullet}/[HEH_2]^{\bullet+}$ is a much weaker acid/base pair than $[ColH]^{+}/HEH_2$.[63] By contrast, rapid unimolecular fragmentations are often required following ET in π-stacked EDA complexes to avoid BET.(41) Once formed, $[Col{-}H]^{\bullet}$ ($BDFE_{N-H,\ estimated}$ = 28 kcal mol^{-1}, see section S11) can transfer an H-atom to substrate (**g**), regenerating Col. Further reactivity of $[HEH]^{\bullet}$ may proceed by direct reduction of the semi-reduced substrate ($subH^{\bullet}$, **h**) or by disproportionation to yield HE and HEH_2 (see Figure D.64 for a representative scheme).

Based on this mechanistic outline, we can rationalize the improved efficiency upon adding Col-buffer. Pre-association of $[ColH]^{+}$ and HEH_2, and subsequent static quenching to produce $ColH^{\bullet}$, decouples substrate reduction from the pre-association step. Instead, forward reduction is determined by the ability to transfer $H^{\bullet}$ from $[Col{-}H]^{\bullet}$ to substrate, which, given the low $BDFE_{N-H}$ (28 kcal mol^{-1}) of $[Col{-}H]^{\bullet}$, will occur for many substrates. This scenario is comparable to the generation of $R^{\bullet}$ from R^{+}-donors and HEH_2, where R = H. Whereas $*HEH_2$ is thermodynamically potent ($BDFE_{C-H}$ = −7 kcal mol^{-1}) for PCET, it is kinetically challenged in terms of productive reactivity. Adding Col-buffer generates a kinetically accessible weak N−H bond. Additionally, the buffer-free reaction is likely also limited by rapid BET between reduced substrates and $[HEH_2]^{\bullet+}$, as $[HEH_2]^{\bullet+}$ is not effectively removed from solution by deprotonation (Figure D.75). This model suggests that while the primary mechanism of $*HEH_2$ oxidation is quenching by acid, the presence of base is also crucial for efficient substrate reduction. The special combination of Col-buffer and HEH_2 in photodriven N_2R (and other reductions discussed herein) can be traced to $[ColH]^{+}$ being a reducible acid with a low propensity for parasitic homocoupling as the reduced radical ($ColH^{\bullet}$) as well as the presence of carbonyl substituents in the 3,5-positions of HEH_2, necessary for H-bonding with $[ColH]^{+}$ in the pre-association step.

An instructive comparison can be made between the excited state reactivity of $*HEH_2$ and a recently developed 12-aryl dihydrobenzoacridine photocatalyst (Figure 5.11A, acrH).[64] Enhanced reducing power is observed for the latter upon addition of an

exogenous base (e.g., MeTBD; MeTBD = 7-Methyl-1,5,7-triazabicyclodecene). A multisite-PCET (MS-PCET) oxidation[65] of the *[acrH] N–H bond, with substrate (e.g., aryl bromides) serving as oxidant, is proposed. Analogously, one can view *HEH_2 reactivity in the presence of Col-buffer as a MS-PCET oxidation of the C–H bond, with $[ColH]^+$ serving as the oxidant and Col as the base (Figure 5.11B, right). While the base is not strictly required to drive the overall transformation (*HEH_2 should readily reduce $[ColH]^+$), it is necessary to circumvent BET.

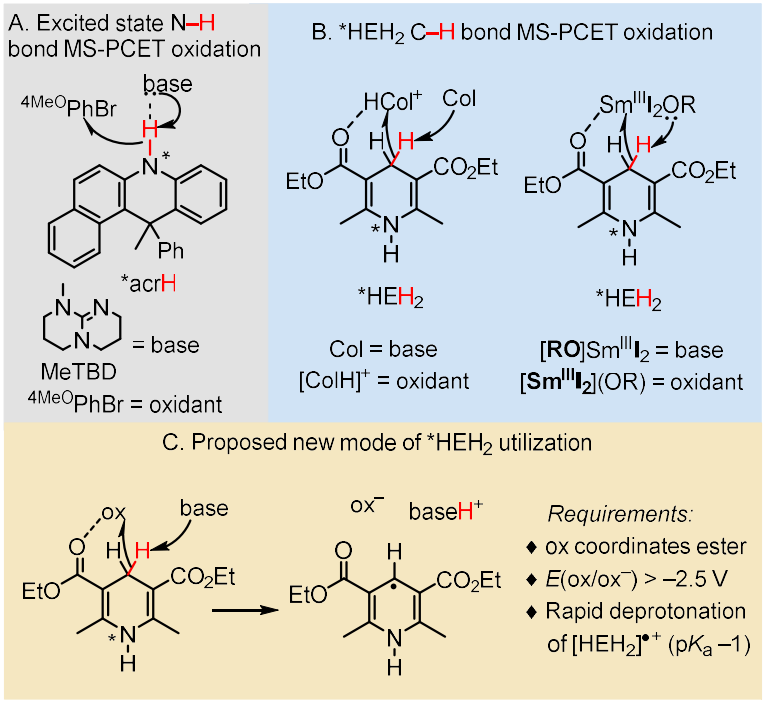

Figure 5.11. A framework for viewing the reactivity of *HEH_2 as the oxidation of the C–H bond relevant to Col-buffer interaction is described and extended to previous work exploring $Sm^{III/II}$ reductions.

In MS-PCET oxidations pre-association of the base with substrate via an acidic X–H bond is typically operative, with the substrate then being oxidized.[66] The carbonyl groups of HEH_2 allow pre-association of the oxidant instead of the base, resulting in oxidation of the less basic *HEH_2 C–H bond. Interestingly, as the C–H bond is oxidized we anticipate a large reorganization energy due to a change in hybridization (sp^3 to sp^2) and a poorer H-bonding interaction with the C-atom of the semi-oxidized species (HEH•).

This should mitigate the rate of back-PCET (in analogy to BET) compared with an O/N−H bond oxidation, resulting in more efficient reduction of $[ColH]^+$ to ColH•.

As an additional point of comparative context, it has been found that $*HEH_2$ can reduce Cr^{III} as well as Sm^{III}-alkoxides (see Chapter 6) to their corresponding divalent metal products and alcohol.[31,35] The photogenerated Sm^{II} and Cr^{II} products can be utilized in Sm-catalyzed cross-coupling and a catalytic-in-Cr Nozaki–Hiyama–Kishi reaction. Initial carbonyl coordination of the Lewis acidic metal ion may be operative in these systems, as observed with $[ColH]^+$ here (Figure 5.11B).

Taken together, these observations point to a new mode for direct reductions by $*HEH_2$ (Figure 5.11C). A Lewis acidic oxidant capable of both coordinating the ester carbonyl functionality and undergoing ET from $*HEH_2$ (E = −2.5 V) is key. Addition of a base helps to avoid BET. Utilizing these simple principles we anticipate the development of photoreductions of oxophilic, redox-active moieties by HEH_2, which in turn may catalyze desired reductive photochemistry.

5.4 Cited References

1. Warren, J. J.; Tronic, T. A.; Mayer, J. M. *Chem. Rev.* **2010**. 110, 6961–7001.
2. Weinberg, D. R.; Gagliardi, C. J.; Hull, J. F.; Murphy, C. F.; Kent, C. A.; Westlake, B. C.; Paul, A.; Ess, D. H.; McCafferty, D. G.; Meyer, T. J. *Chem. Rev.* **2012**. 112, 4016–4093.
3. Murray, P. R. D.; Cox, J. H.; Chiappini, N. D.; Roos, C. B.; McLoughlin, E. A.; Hejna, B. G.; Nguyen, S. T.; Ripberger, H. H.; Ganley, J. M.; Tsui, E.; Shin, N. Y.; Koronkiewicz, B.; Qiu, G.; Knowles, R. R. *Chem. Rev.* **2022**. 122, 2017–2291.
4. Tyburski, R.; Liu, T.; Glover, S. D.; Hammarström, L. *J. Am. Chem. Soc.* **2021**. 143, 560–576.
5. Chalkley, M. J.; Garrido-Barros, P.; Peters, J. C. *Science* **2020**. 369, 850–854.
6. Lennox, J. C.; Kurtz, D. A.; Huang, T.; Dempsey, J. L. *ACS Energy Lett.* **2017**. 2, 1246–1256.

7. Wenger, O. S. *Chem. – Eur. J.* **2011**. 17, 11692–11702.
8. Wenger, O. S. *Acc. Chem. Res.* **2013**. 46, 1517–1526.
9. Pannwitz, A.; Wenger, O. S. *Phys. Chem. Chem. Phys.* **2016**. 18, 11374–11382.
10. Barrett, S. M.; Pitman, C. L.; Walden, A. G.; Miller, A. J. M. *J. Am. Chem. Soc.* **2014**. 136, 14718–14721.
11. Park, Y.; Kim, S.; Tian, L.; Zhong, H.; Scholes, G. D.; Chirik, P. J. *Nat. Chem.* **2021**. 13, 969–976.
12. Kim, S.; Park, Y.; Kim, J.; Pabst, T. P.; Chirik, P. J. *Nat. Synth.* **2022**. **1**, 297–303.
13. Park, Y.; Tian, L.; Kim, S.; Pabst, T. P.; Kim, J.; Scholes, G. D.; Chirik, P. J. *JACS Au* **2022**. 2, 407–418.
14. Garrido-Barros, P.; Romero, C. G.; Winkler, J. R.; Peters, J. C. *J. Am. Chem. Soc.* **2024**. 146, 12750–12757.
15. Johansen, C. M.; Boyd, E. A.; Peters, J. C. *Sci. Adv.* **2022**. 8, eade3510.
16. Ashida, Y.; Onozuka, Y.; Arashiba, K.; Konomi, A.; Tanaka, H.; Kuriyama, S.; Yamazaki, Y.; Yoshizawa, K.; Nishibayashi, Y. *Nat. Commun.* **2022**. 13, 7263.
17. Arashiba, K.; Miyake, Y.; Nishibayashi, Y. *Nat. Chem.* **2011**. 3, 120–125.
18. Arashiba, K.; Eizawa, A.; Tanaka, H.; Nakajima, K.; Yoshizawa, K.; Nishibayashi, Y. *Bull. Chem. Soc. Jpn.* **2017**. 90, 1111-1118.
19. Ashida, Y.; Arashiba, K.; Nakajima, K.; Nishibayashi, Y. *Nature* **2019**. 568, 536–540.
20. Chalkley, M. J.; Drover, M. W.; Peters, J. C. *Chem. Rev.* **2020**. 120, 5582–5636.
21. Shen, G.-B.; Fu, Y.-H.; Zhu, X.-Q. *J. Org. Chem.* **2020**. 85, 12535–12543.
22. Konev, M. O.; Cardinale, L.; Jacobi von Wangelin, A. *Org. Lett.* **2020**. 22, 1316–1320.
23. Singh, S.; Sharma, V. K.; Gill, S.; Sahota, R. I. K. *J. Chem. Soc. Perkin 1,* **1985**. 0, 437–440 (1985).
24. Jung, J.; Kim, J.; Park, G.; You, Y.; Cho, E. J. *Adv. Synth. Catal.* **2016**. 358, 74–80.

25. Ohnishi, Y.; Kagami, M.; Ohno, A. *Chem. Lett.* **1975**. 4, 125–128.
26. Deng, G.; Xu, H.-J.; Chen, D.-W. *J. Chem. Soc., Perkin Trans. 2,* **1990**. 7, 1133–1137.
27. Wu, J.; Grant, P. S.; Li, X.; Noble, A.; Aggarwal, V. K. *Angew. Chem. Int. Ed.* **2019**. 58, 5697–5701.
28. Kammer, L. M.; Badir, S. O.; Hu, R.-M.; Molander, G. A. *Chem. Sci.* **2021**. 12, 5450–5457.
29. Li, J.; Siang Tan, S.; Kyne, S. H.; Wai Hong Chan, P. *Adv. Synth. Catal.* **2022**. 364, 802–810.
30. Suresh Yedase, G.; Venugopal, S.; P., A.; Reddy Yatham, V. *Asian J. Org. Chem.* **2022**. 11, e202200478.
31. Liu, Y.; Lin, S.; Zhang, D.; Song, B.; Jin, Y.; Hao, E.; Shi, L. *Org. Lett.* **2022**. 24, 3331–3336.
32. Bergamaschi, E.; Mayerhofer, V. J.; Teskey, C. J. *ACS Catal.* **2022**. 12, 14806–14811.
33. Ji, C.-L.; Han, J.; Li, T.; Zhao, C.-G.; Zhu, C.; Xie, J. *Nat. Catal.* **2022**. 5, 1098–1109.
34. Buzzetti, L.; Prieto, A.; Roy, S. R.; Melchiorre, P. *Angew. Chem. Int. Ed.* **2017**. 56, 15039–15043.
35. Johansen, C. M.; Boyd, E. A.; Tarnopol, D. E.; Peters, J. C. *J. Am. Chem. Soc.* **2024**. 146, 25456–25461.
36. Buzzetti, L.; Prieto, A.; Roy, S. R.; Melchiorre, P. *Angew. Chem. Int. Ed.* **2017**. 56, 15039–15043.
37. van Leeuwen, T.; Buzzetti, L.; Perego, L. A.; Melchiorre, P. A. *Angew. Chem. Int. Ed.* **2019**. 58, 4953–4957.
38. Wang, K.; Bao, X. *J. Am. Chem. Soc.* **2024**. 146, 7679–7689.
39. Coohill, T. P. *Photochem. Photobiol.* **1991**. 54, 859–870.

40. Eizawa, A.; Arashiba, K.; Tanaka, H.; Kuriyama, S.; Matsuo, Y.; Nakajima, K.; Yoshizawa, K.; Nishibayashi, Y. *Nat. Commun.* **2017**. 8, 14874.
41. Wortman, A. K.; Stephenson, C. R. J. . *Chem* **2023**. 9, 2390–2415.
42. Pitre, S. P.; Allred, T. K.; Overman, L. E. *Org. Lett.* **2021**. 23, 1103–1106.
43. Zega, A.; Srčič, S.; Mavri, J.; Bešter-Rogač, M. *J. Mol. Struct.* **2008**. 875, 354–363.
44. Tao, J.; Perdew, J. P.; Staroverov, V. N.; Scuseria, G. E. *Phys. Rev. Lett.* **2003**. 91, 146401–146404.
45. Weigend, F. *Phys. Chem. Chem. Phys.* **2006**. 8, 1057–1065.
46. Barone, V.; Cossi, M. *J. Phys. Chem. A* **1998**. 102, 1995–2001.
47. Lakowicz, J. R., *Principles of Fluorescence Spectroscopy*. **2006** Springer.
48. Czochralska, B.; Lindqvist, L. *Chem. Phys. Lett.* **1983**. 101, 297–299.
49. Anne, A.; Hapiot, P.; Moiroux, J.; Neta, P.; Saveant, J. M. *J. Am. Chem. Soc.* **1992**. 114, 4694–4701.
50. Zielonka, J.; Marcinek, A.; Adamus, J.; Gębicki, J. *J. Phys. Chem. A* **2003**. 107, 9860–9864.
51. Fukuzumi, S.; Koumitsu, S.; Hironaka, K.; Tanaka, T. *J. Am. Chem. Soc.* **1987**. 109**,** 305–316.
52. Munisamy, T.; Schrock, R. R. *Dalton Trans.* **2011**. 41, 130–137.
53. Cheng, T.; Shen, D. X.; Meng, M.; Mallick, S.; Cao, L.; Patmore, N. J.; Zhang, H. L.; Zou, S. F.; Chen, H. W.; Qin, Y.; Wu, Y. Y.; Liu, C. Y. *Nat. Commun.* **2019**. 10, 1531.
54. de Rege, P. J. F.; Williams, S. A.; Therien, M. J. *Science* **1995**. 269, 1409–1413.
55. Yan, T.; Yang, J.; Yan, K.; Wang, Z.; Li, B.; Wen, J. *Angew. Chem. Int. Ed.* **2024**. 63, e202405186.
56. Tshepelevitsh, S.; Kütt, A.; Lõkov, M.; Kaljurand, I.; Saame, J. ; Heering, A.; Plieger, P. G.; Vianello, R.; Leito, I. *Eur. J. Org. Chem.* **2019**. 2019, 6735–6748.
57. Zeldes, H.; Livingston, R. *J. Magn. Reson. (1969)* **1979**. 34, 543–552.

58. Dohrmann, J. K.; Becker, R. *J. Magn. Reson. (1969)* **1977**. 27, 371–384.
59. Cao, K.; Tan, S. M.; Lee, R.; Yang, S.; Jia, H.; Zhao, X.; Qiao, B.; Jiang, Z. *J. Am. Chem. Soc.* **2019**. 141, 5437–5443.
60. Golubev, N. S.; Smirnov, S. N.; Schah-Mohammedi, P.; Shenderovich, I. G.; Denisov, G. S.; Gindin, V. A.; Limbach, H. H. *Russ. J. Gen. Chem.* **1997**. 67, 1082–1087.
61. Boyd, E. A.; Peters, J. C. *J. Am. Chem. Soc.* **2022**. 144, 21337–21346.
62. Zhang, J.; Mück-Lichtenfeld, C.; Studer, A. *Nature* **2023**. 619, 506–513.
63. Zhao, G.-J.; Han, K.-L. *Acc. Chem. Res.* **2012.** 45, 404–413.
64. Bortolato, T.; Simionato, G.; Vayer, M.; Rosso, C.; Paoloni, L.; Benetti, E. M.; Sartorel, A.; Lebœuf, D.; Dell'Amico, L. *J. Am. Chem. Soc.* **2023**. 145, 1835–1846.
65. Darcy, J. W.; Koronkiewicz, B.; Parada, G. A.; Mayer, J. M. *Acc. Chem. Res.* **2018**. 51, 2391–2399.
66. Morton, C. M.; Zhu, Q.; Ripberger, H.; Troian-Gautier, L.; Toa, Z. S. D.; Knowles, R. R.; Alexanian, E. J. *J. Am. Chem. Soc.* **2019**. 141, 13253–13260.